Data repository materials associated with *A matter of minutes: Breccia dike paleomagnetism provides evidence for rapid crater modification*

This document is provided as the data repository for a Geology article entitled **A matter of minutes: Breccia dike paleomagnetism provides evidence for rapid crater modification** by Luke M. Fairchild, Nicholas L. Swanson-Hysell and Sonia M. Tikoo.

This document has been modified from interactive Jupyter notebooks in which the data analysis below is carried out using Python code. Full digital versions of these notebooks, including all code and data files, are available for download and interactive viewing from this GitHub repository: https://github.com/Swanson-Hysell-Group/2016_Breccia_Dikes. Running the code in the notebooks requires a standard scientific Python distribution and the open-source PmagPy software package (https://github.com/PmagPy/; Tauxe et al., 2016). The version of PmagPy used at the time these notebooks were made is also available for download within the GitHub repository.

These notebooks can also be viewed in two statically rendered websites:

- **Paleomagnetic Data Analysis:**
  https://nbviewer.jupyter.org/github/swanson-hysell-group/2016_Breccia_Dikes/blob/master/Code/Breccia_Dike_Data.ipynb
- **Breccia Dike Cooling Model:**
  https://nbviewer.jupyter.org/github/swanson-hysell-group/2016_Breccia_Dikes/blob/master/Code/dike_cooling_model.ipynb

1 Breccia Dike Descriptions

PI47 breccia dike Site PI47 is a clast-poor breccia dike intruding Archean schist that is approximately 3–4 cm thick (Fig. S1L). The site PI47 sample collection comprises nine samples of green-colored matrix. Core samples are 2.5 cm in diameter and therefore span most of the breccia dike's width as seen in the photo below. The parameters used in the breccia dike cooling model are from this site, as its minimal thickness is a useful boundary condition for determining the maximum timeframe in which the breccia dike impact direction (ChRM) was recorded.

DeI2 breccia dike At site DeI2, the matrix of a 2 to 8 cm thick breccia dike was sampled. The matrix is composed of hematite-rich siltstone (Fig. S1A). Clasts were sub-angular to sub-rounded fine to very coarse grained sand grains, and consisted dominantly of quartz with the minor presence of red and gray lithics.

PI2 breccia dike Breccia dike PI2 contained clasts of amygdaloidal basalt as well as more massive mafic volcanics some with hematite alteration. The largest sampled clast was 17×14 cm. The matrix at this site was a deep red color, likely a consequence of interstitial hematite (Fig. S1C).

Paleomagnetic directions of clasts exhibit a low coercivity remanence that fails a conglomerate test and aligns well with the impact direction inferred from other breccia sites. The high coercivity

components, on the other hand, are quite scattered and suggest that clasts at this site were not fully remagnetized. Unfortunately, these clast samples experienced intense gyroremanence during AF demagnetization, so a separate high coercivity component was not well isolated. Additionally, there was not enough remaining sample material for thermal demagnetization. We present the low coercivity data here as a likely partial TRM acquired during emplacement (if not a full TRM that was obscured by GRM during measurement). Clast sample PI2c-1a (amygdaloidal basalt) is shown in Figure S1B.

PI15 breccia dike At site PI15, the matrix of a 20 cm thick breccia dike was sampled. The matrix is green/grey and contains small (mm-scale) clasts (Fig. S1D).

PI16 breccia dike At site PI16, 25 clasts of Archean schist were sampled within an up to 80 cm thick breccia dike (Fig. S1E).

PI22 breccia dike At site PI22, 15 clasts comprised of felsic porphyry—with the exceptions of samples PI22-1 and PI22-2 (felsic metamorphic schist) and PI22-3 (intermediate metavolcanic)—were sampled within an ∼10 m thick breccia dike (Fig. S1F). Clasts are subangular, and sampled clasts range in size from 9 to 40 cm in diameter.

PI24 breccia dike At site PI24, 8 clasts comprised of Archean felsic intrusive rock (PI24c-1 through PI24c-8) were sampled from a 1.4 m wide breccia dike (Fig. S1G). Clasts are subangular and range from granule size to 50 cm in length. Multiple clasts contain shatter cones, indicating emplacement subsequent to the passing of the shock wave. The breccia matrix is gray/green. PI24m-9 through PI24m-14 are matrix samples.

PI26 breccia dike At site PI26, 8 samples of matrix were collected from a breccia dike network intruding felsic Archean schist (Fig. S1H). The multiple diverging branches of the breccia dike are up to 40 cm thick. Branches thin to mm-scale thickness farther away from the locus of the breccia network. The breccia dike is clast-rich, but matrix-supported. Clasts are angular to subangular, granule to pebble size, and are comprised of a variety of metamorphic lithologies and some diabase. Some clasts are of the same lithology as the adjacent host rock, but others are not from the immediate locale. The breccia dike matrix is fine to very fine grained and its dark red coloration due to the presence of interstitial hematite.

PI31 breccia dike At the site PI31 breccia dike, 20 clasts comprised of felsic, mafic, and K-feldspar porphyry schist were sampled from a >3 m breccia dike (Fig. S1I). The matrix of the breccia is a deep red color.

PI44 breccia dike At site PI44, 13 samples of matrix were collected from a ∼10-40 cm thick breccia dike (Fig. S1J). The breccia cross-cuts a Keweenawan diabase dike and an Archean schist. Clasts are dominantly pebble size, but can be as large as 25 cm in length. The breccia matrix is fine-grained and the collected specimens include small, granule-sized clasts.

PI46 breccia dike At site PI46, 11 samples of matrix were collected from a 25 cm thick breccia dike (Fig. S1K). The breccia dike contains granule to small-sized clasts (the largest clast is 15 cm across, although the majority are smaller). The breccia matrix is green/gray and very fine-grained.

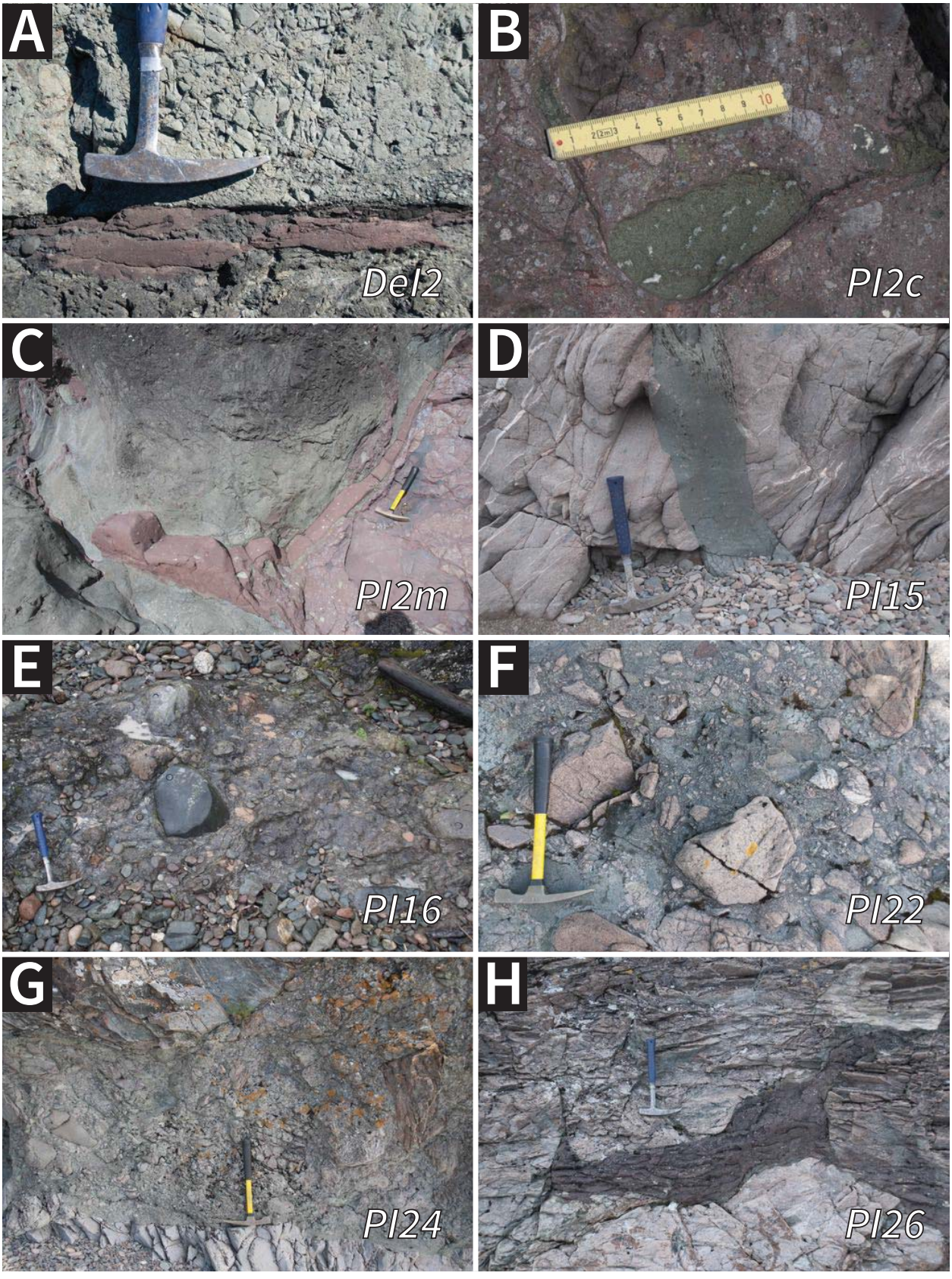
A
Del2
B
Pl2c
C
Pl2m
D
Pl15
E
Pl16
F
Pl22
G
Pl24
H
Pl26

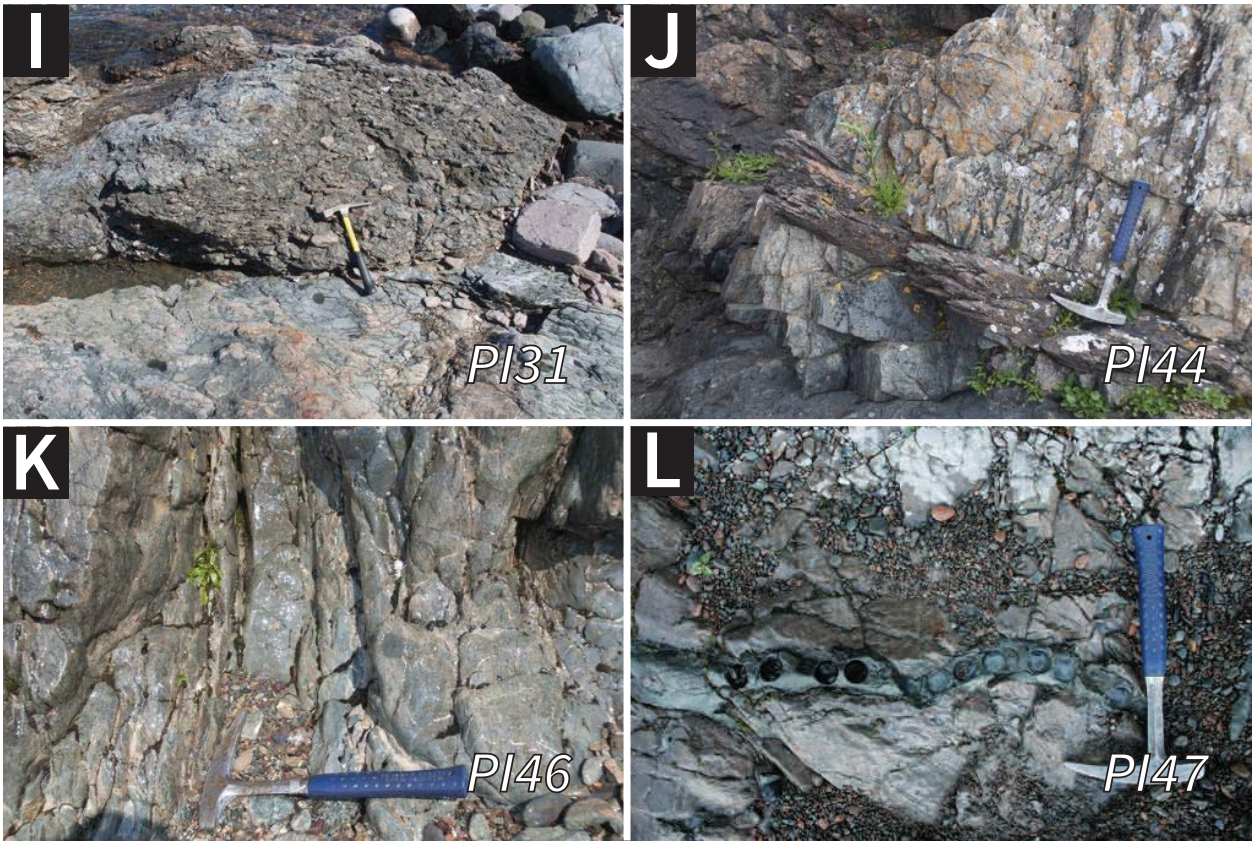

Figure S1. Field photographs of lithic breccia dike sample sites labeled by site name. Clast sample PI2c–1a (amygdaloidal basalt) is pictured in B (10 cm ruler for scale).

2 Breccia Dike Paleomagnetic Analysis

2.1 Paleomagnetic Results

Directional fits were made to paleomagnetic data using least-squares analysis (Kirschvink, 1980) using the software package PmagPy (`https://github.com/PmagPy/`). Raw data in both CIT and MagIC formats can be found in the `Data` folder of the GitHub repository. Data are also available in the MagIC database (`http://earthref.org/MagIC/11292/`). Individual samples within the sites listed below can contain anywhere from a single to several directional components. For thermal demagnetization data, the abbreviations for each component (signifying the blocking temperatures over which they were fit) are:

- **HT** High temperature — 450 to 580 °C
- **LT/PLF** Low temperature — NRM to 300–400 °C
- **hem** Hematite — 580 to $\leq$ 680 °C

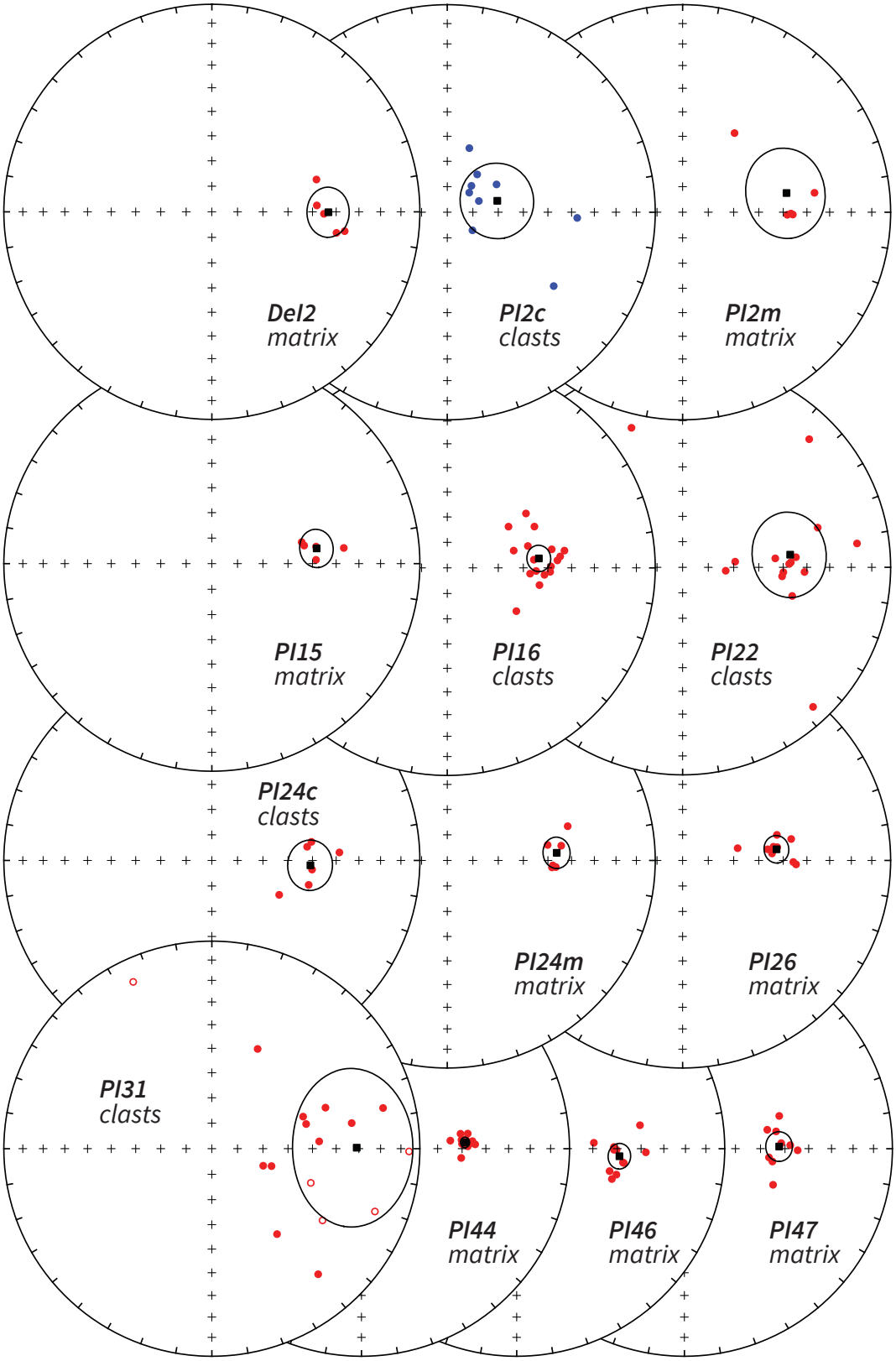

Figure S2. ChRM directions of breccia dike samples and associated site means (black square with α_{95} error radius). Solid dots plot in the lower hemisphere and open dots in the upper. Red (blue) dots are sample magnetization directions from least-squares fits to thermal (AF) demagnetization data. Except in the case of PI2c (AF data), all directions shown are 'HT' fits.

2.2 Conglomerate Test Results

Conglomerate tests were performed on clast samples from sites PI16, PI22, PI24, and PI31. To determine whether breccia dike clasts were remagnetized during their emplacement, we test for the null hypothesis of randomness among their paleomagnetic directions. In the Watson test for randomness, if a resultant vector length (R) for a population of unit vectors exceeds a specified length (R_o) then the null hypothesis of randomness can be rejected. Watson (1956) shows that R_o can be calculated as: $R_o = \sqrt{(7.815 * N/3)}$. In paleomagnetism, the Watson randomness test is commonly referred to as a conglomerate test.

All breccia dike sites where clasts were sampled failed a paleomagnetic conglomerate test at the 99% confidence level (see table below) indicating that the directions are non-random.

Table S1. Conglomerate test results from breccia dike sites where clasts were sampled.

	Demag type	n	R	R_0	result	95% confidence	99% confidence
PI2c	AF	17	8.6718	6.251000	FAIL	YES	YES
PI16	Thermal	17	16.7069	6.251000	FAIL	YES	YES
PI22	Thermal	15	12.9965	6.251000	FAIL	YES	YES
PI24c	Thermal	6	5.9056	3.953479	FAIL	YES	YES
PI31	Thermal	16	10.6733	6.251000	FAIL	YES	YES

2.3 Site Means

A couple of the site means have quite large α_{95} uncertainties and although they correspond with the mean population, we consider it best to filter them out of the calculation of an overall mean of the sites. Only sites with α_{95}<16° are included in the calculation of the overall mean.

Table S2. Paleomagnetic site means for all breccia dike sample locations.

	Site type	Site Lat (°N)	Site Lon (°E)	Demag type	Dec	Inc	α_{95}	n	κ	R
PI47	breccia dike matrix	48.7	-87.0	Thermal	88.7°	52.4°	5.5°	9	90	8.91
DeI2	breccia dike matrix	48.7	273.0	Thermal	90.2°	43.3°	9.0°	5	73	4.94
PI2c	breccia dike clasts	48.6	272.9	AF	77.1°	69.9°	14.6°	9	13	8.39
PI2m	breccia dike matrix	48.6	272.9	Thermal	79.5°	47.9°	16.6°	5	22	4.82
PI15	breccia dike matrix	48.6	273.0	Thermal	81.7°	47.8°	7.0°	5	119	4.96
PI16	breccia dike clasts	48.7	273.0	Thermal	84.1°	53.5°	4.9°	17	55	16.70
PI22	breccia dike clasts	48.7	273.0	Thermal	83.3°	46.8°	15.6°	15	7	12.99
PI24c	breccia dike clasts	48.7	273.0	Thermal	92.8°	50.8°	9.3°	6	53	5.90
PI24m	breccia dike matrix	48.7	273.0	Thermal	86.0°	46.2°	5.7°	6	140	5.96

PI26	breccia dike matrix	48.6	273.0	Thermal	83.2°	52.5°	5.1°	9	103	8.92
PI31	breccia dike clasts	48.6	273.0	Thermal	89.6°	31.0°	27.2°	16	3	10.67
PI44	breccia dike matrix	48.7	272.9	Thermal	86.5°	48.7°	1.9°	12	499	11.97
PI46	breccia dike matrix	48.7	273.0	Thermal	94.2°	49.0°	4.7°	11	96	10.89
Grand mean†					86.59°	51.05°	4.28°	11	114.8	10.9

† Grand mean is calculated from thermal demagnetization data only and site means with α_{95}<16°.

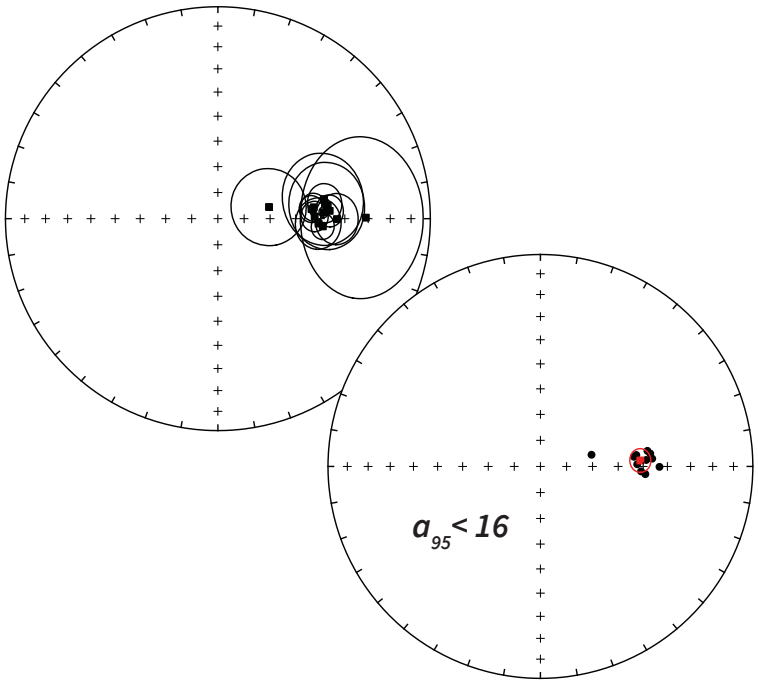

Figure S3. Equal area plots of breccia dike site means. The left plot displays all site means with their α_{95} errors. The right plot shows only site means with $\alpha_{95} < 16.0$ and their overall mean with error (red).

2.4 Breccia dike host rock

Here we present the results of baked contact tests for one breccia dike intrusion into a stack of basalt flows (host rock sites PI32, PI33, PI34) and three breccia dike intrusions into Archean schist (host rock sites PI16, PI22, PI24). These results support the hypothesis that breccia dikes were emplaced at high temperatures, which imparted partial overprints to host rock removed at lower (higher) temperatures at greater (lesser) distance from the nearest breccia dike contact. Moreover, the general observation of partial overprinting of host rock (pTRM) contrasts with the full overprinting of daughter clasts of similar lithology within breccia dikes and therefore supports the hypothesis that breccia dike clasts record a TRM.

The maximum unblocking temperatures of magnetic components have been compiled for both breccia dike clasts and host rock data. We first initialize the plot we will use to visualize the baked

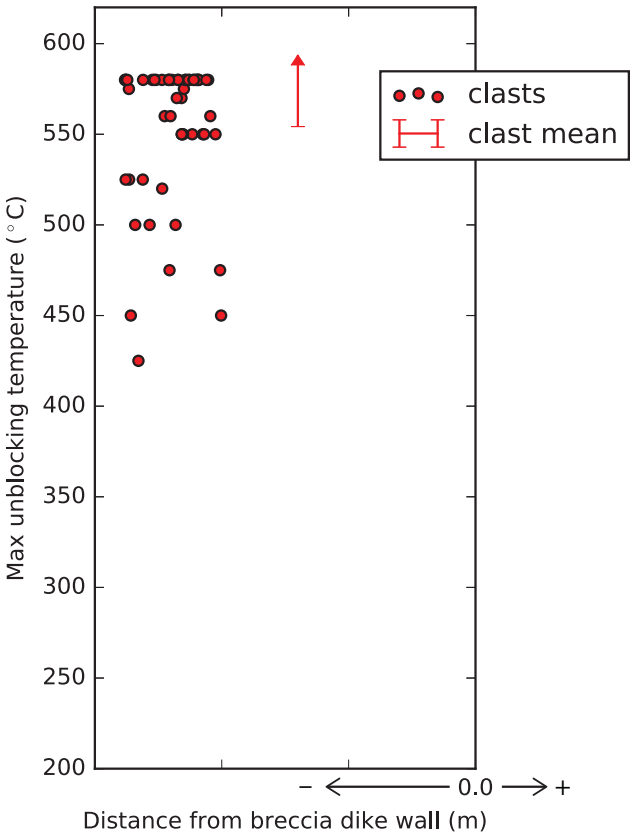

Figure S4. Unblocking temperatures of impact directions from all breccia dike clasts sampled in this study, plotted against distance from breccia dike wall (negative distance). Temperature data are plotted in such a way as to be a visual reference for the baked contact tests in Figures S5 and S8. No scale is provided for the horizontal axis as these particular data were not collected; the horizontal scatter is only to prevent overlap of points.

contact test and compare the unblocking temperatures to distance from the nearest breccia dike. We start by plotting the range of temperatures at which the full overprints in breccia dike clasts were removed from clasts throughout the sampled breccia dikes (Fig. S4). This range will be used as a helpful visual comparison in the baked contact tests to follow.

2.4.1 PI32, PI33 and PI34 host rock sites

In a stratigraphic section of Keweenawan lava flows, sites PI32 and PI33 are from flows that are ∼22 meters and ∼18 meters respectively away from a ∼5 meter thick breccia dike. PI34 is from the flow that is in contact with that ∼5 meter breccia dike with samples within a dike width's distance. PI32 and PI33 have partial impact direction overprints removed at ∼275 °C while PI34 is fully overprinted in the impact direction (Fig. S5). We interpret these PI34 results to indicate that the complete overprint of the samples is associated with localized heating due to emplacement of the hot breccia dike while the partial overprint on PI32 and PI33 is due to regionally elevated temperatures. These results constitute a positive test of the hypothesis that breccia dikes were emplaced hot into cooler rock and subsequently conductively cooled.

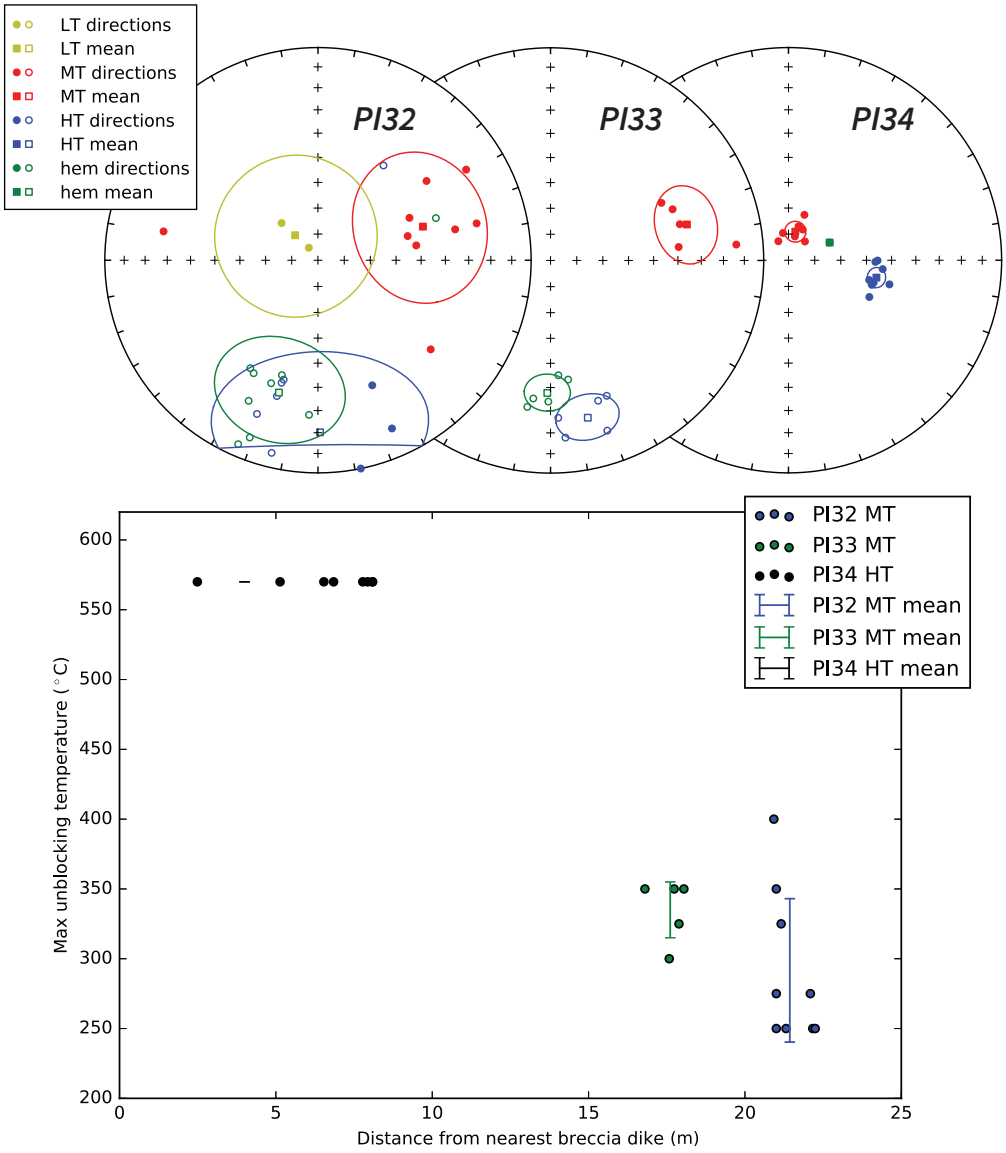

Figure S5. Equal area plots of magnetization component directions of basalt sites PI32, PI33, and PI34. PI34 hosts a breccia dike intrusion. The lower diagram plots the maximum unblocking temperature of impact-direction overprints within basalt host rock against distance from the breccia dike that intrudes flow PI34. This plot demonstrates a positive baked contact test.

2.4.2 Archean schist

Here we present paleomagnetic data of breccia dike host rock (Archean schist) obtained from three breccia dike sample sites. In addition to Archean schist being poor magnetic recorders with the potential to have 1) pTRM tails that cause remanence to be blocked at higher temperatures and 2) weak pre-impact remanence, the occasional high variability of unblocking temperatures may be due to the fact that the distance from the nearest breccia dike assigned to each data point is often unclear. Breccia dike networks are complicated and may extend closer to our host rock sampling sites than we are able to observe; it is also possible that initial breccia dike/host rock contacts have since been eroded. These factors may be responsible for outliers in Figure S8. Regardless, a relationship between the magnetizations of breccia dike clasts (plotted in red at a negative distance)

and their parent (host) rocks can be established from the data (Fig. S8). The impact direction magnetizations of host rock are consistently removed at temperatures below 580 °C (Fig. S7) when sampled at appreciable distance from a breccia dike intrusion, indicating that the impact direction in host rocks is a partial thermal overprint (pTRM) as opposed to the full TRM acquired by breccia dike clasts.

PI16 host rock At site PI16, 5 samples of mafic to intermediate Archean greenschist were collected at a minimum distance of 8 m from the nearest exposed breccia dike, which was approximately 0.4 meters thick. The demagnetization data reveal that these samples have a present local field overprint, a partial impact direction overprint and a poorly resolved direction held at unblocking temperatures above those that remove the impact direction. These results supports the interpretation that heating to temperatures >580 °C was localized to the breccia dikes and their immediate vicinity.

PI22 host rock At breccia dike site PI22, 16 samples of Archean mafic schist host rock were collected at variable distances (3 cm to >5 m) from the nearest observable breccia dike contact. The thickness of breccia dike PI22 varied from 0.75–1.3 meters in the vicinity of the baked contact test.

PI24 host rock At breccia dike site PI24, 15 samples of K-feldspar porphyry host rock were sampled at variable distances (4 cm to >3 m) from the closest observable breccia dike contact. Figure S6 shows the sharp contact (outlined in yellow) of the breccia dike intrusion (top) with the host rock (bottom) that was amenable to a baked contact test. The thickness of breccia dike PI24 varied from 2.2–2.6 meters in the vicinity of the baked contact test.

Figure S6. Breccia dike/host rock contact (outlined in yellow) at sample site PI24.

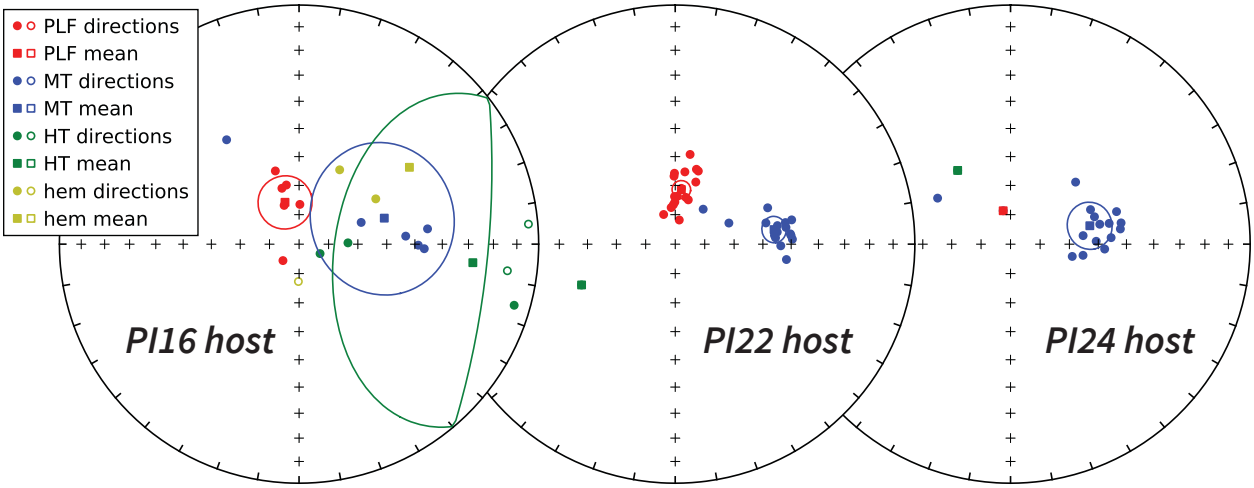

Figure S7. Equal area plots of magnetization component directions of host rock from breccia dike sites PI16, PI22, and PI24. Among the resolvable paleomagnetic directions of breccia dike host rock, the component labeled **MT** (mid-temperatures) is most representative of the Slate Islands impact direction recorded in breccia dikes.

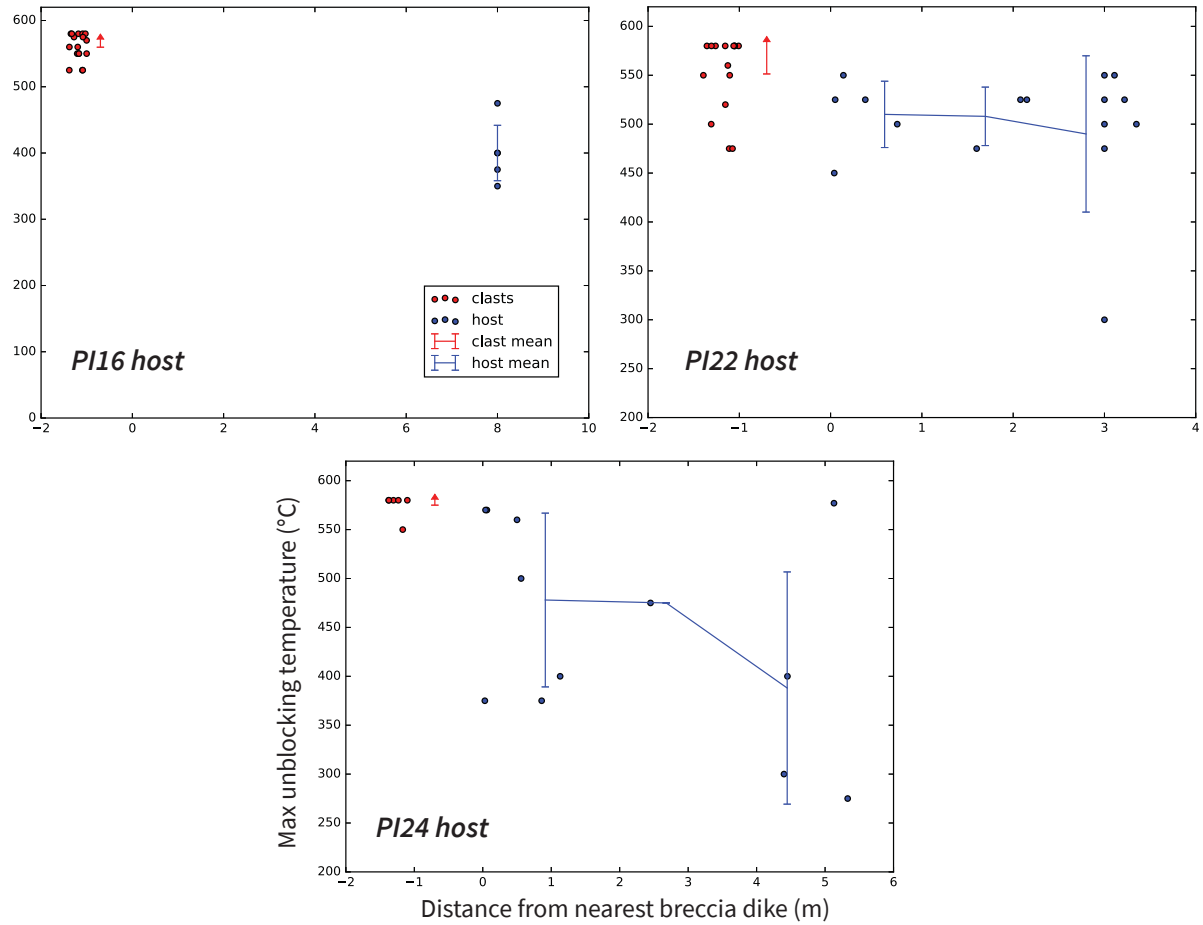

Figure S8. Maximum unblocking temperatures of MT magnetization component from Archean schist host rock plotted as a function of distance from nearest breccia dike intrusion.

2.5 Clasts/Matrix Comparison

The means of both clast and matrix sample sites are compiled and filtered ($\alpha_{95} < 16.0$) in Figure S9.

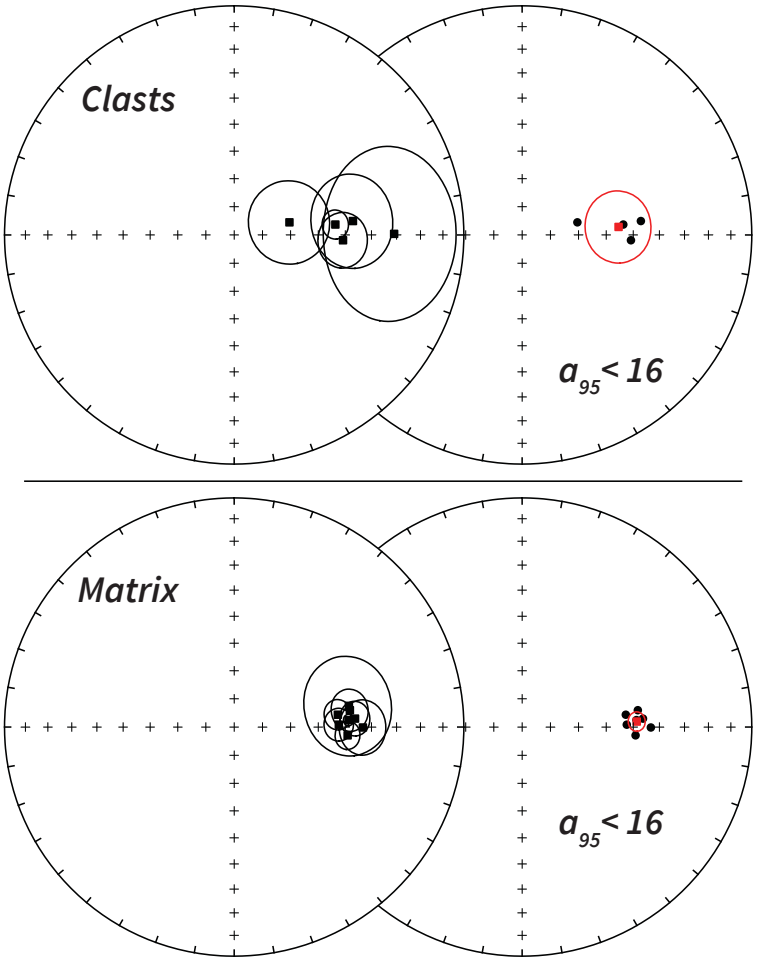

Figure S9. Paleomagnetic site means for clast and matrix samples. Equal area plots to the right display all site means with α_{95} errors, while those to the right display filtered site means with the overall mean and its error (red).

In Figure S10 we see that both clasts and matrix yield a common mean. We exclude clast sites **PI2c** and **PI31** from the overall mean given the irregularity of the AF data for site PI2c and large α_{95} for PI31. Note that PI31 still fails a conglomerate test at the 99% confidence level despite its large α_{95}.

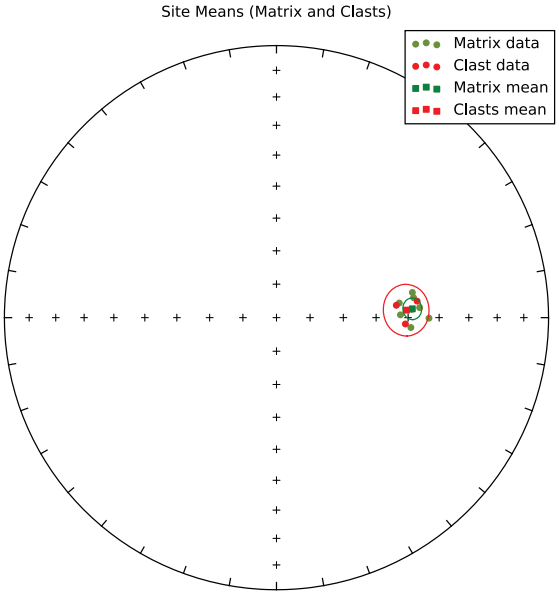

Figure S10. Site means separated by matrix and clast sample sites with their respective overall means.

2.6 Overall Mean

We calculate an overall mean paleomagnetic direction for breccia dikes in the Slate Islands that combines the matrix and clast results. This direction can be considered to be the Slate Islands "impact direction" (Dec=86.4°, Inc=49.1°, α_{95}=2.4°; Table S2), and is shown in Figure 2B of the main text.

3 Virtual Geomagnetic Pole Calculations

3.1 VGP Calculations and Mean Pole

Table S3. Virtual geomagnetic poles (VGPs) calculated for each breccia dike site.

	site type	VGP Lat (°N)	VGP Lon (°E)	Reversed Lat	Reversed Lon
PI47	breccia dike matrix	24.939599	340.629082	-24.939599	160.629082
DeI2	breccia dike matrix	18.549815	345.588504	-18.549815	165.588504
PI2c*	breccia dike clasts	43.828671	325.841478	-43.828671	145.841478
PI2m	breccia dike matrix	27.945514	349.775862	-27.945514	169.775862
PI15	breccia dike matrix	26.475001	348.474455	-26.475001	168.474455
PI16	breccia dike clasts	28.478517	342.659758	-28.478517	162.659758
PI22	breccia dike clasts	24.900680	348.126813	-24.900680	168.126813
PI24c	breccia dike clasts	21.417962	339.161877	-21.417962	159.161877
PI24m	breccia dike matrix	22.839605	346.699576	-22.839605	166.699576
PI26	breccia dike matrix	28.366994	343.989806	-28.366994	163.989806
PI31*	breccia dike clasts	12.723598	352.051585	-12.723598	172.051585
PI44	breccia dike matrix	23.992766	344.617234	-23.992766	164.617234

PI46	breccia dike matrix	19.431098	339.451746	-19.431098	159.451746
Mean pole: 24.34° N, 344.43° E, $A_{95} = 2.7°$					

* Sites not used in calculation of mean pole

From the clast sites in Table S3, we select sites **PI16**, **PI22**, and **PI24c** based on $\alpha_{95} < 16.0$ and reliability of demagnetization data (irregular AF demagnetization data of PI2c was rejected for the final analysis). All matrix sites above were selected for the final VGP analysis. The resulting mean pole is given in Table S3 and plotted in Figure S11.

Figure S11. VGPs and mean poles prior to (inset globe: 'All data') and after (larger globe) filtering.

3.2 Comparison to Laurentia APWP

Given the quickly-acquired nature of magnetizations in lithic breccia dikes within the Slate Islands impact structure, the calculated VGP does not average out geomagnetic secular variation. As a result, it is difficult to correlate it to apparent polar wander paths (APWPs) with high confidence. Nevertheless, such a comparison can be valuable as VGPs tend to be close to mean poles. Given the interpretation from Ar-Ar dating of pseudotachylite impact melt (Dressler et al., 1999) that the impact event occurred at ca. 440 Ma, the lithic breccia dike VGP (from this study and as calculated in Halls, 1979) is compared to poles from the Phanerozoic APWP as compiled by Torsvik et al. (2012). Figure S12A shows this comparison with poles color-coded by age and reveals a ~47° difference between the Slate Islands VGP and the Silurian paleopole that most closely corresponds in age to the 440 Ma age assigned to the Slate Islands impact by Dressler et al. (1999). The Slate

Islands VGP is ∼35° from the ca. 490 Ma Oneota Dolomite pole. Halls (1979) noted the similarity of the Slate Islands VGP to the late Meso- to Neoproterozoic "Grenville Loop" of the Laurentia APWP. Figure S12B compares the Slate Islands VGP (reversed polarity) to the Proterozoic APWP of Laurentia as compiled by Swanson-Hysell et al. (2012). We see that the Slate Islands lithic breccia dike VGP matches better with the late Mesoproterozoic portion of the Laurentia APWP than the Paleozoic (Silurian) portion, despite radiometric evidence for a ∼440 Ma impact age (Dressler et al., 1999). To address the apparent disagreement between the radiometric Silurian age of the crater and its paleomagnetic direction, we next investigate the likelihood of a >30° or >40° geomagnetic excursion as would be implied by the difference between the Slate Islands VGP and the Paleozoic APWP of Laurentia.

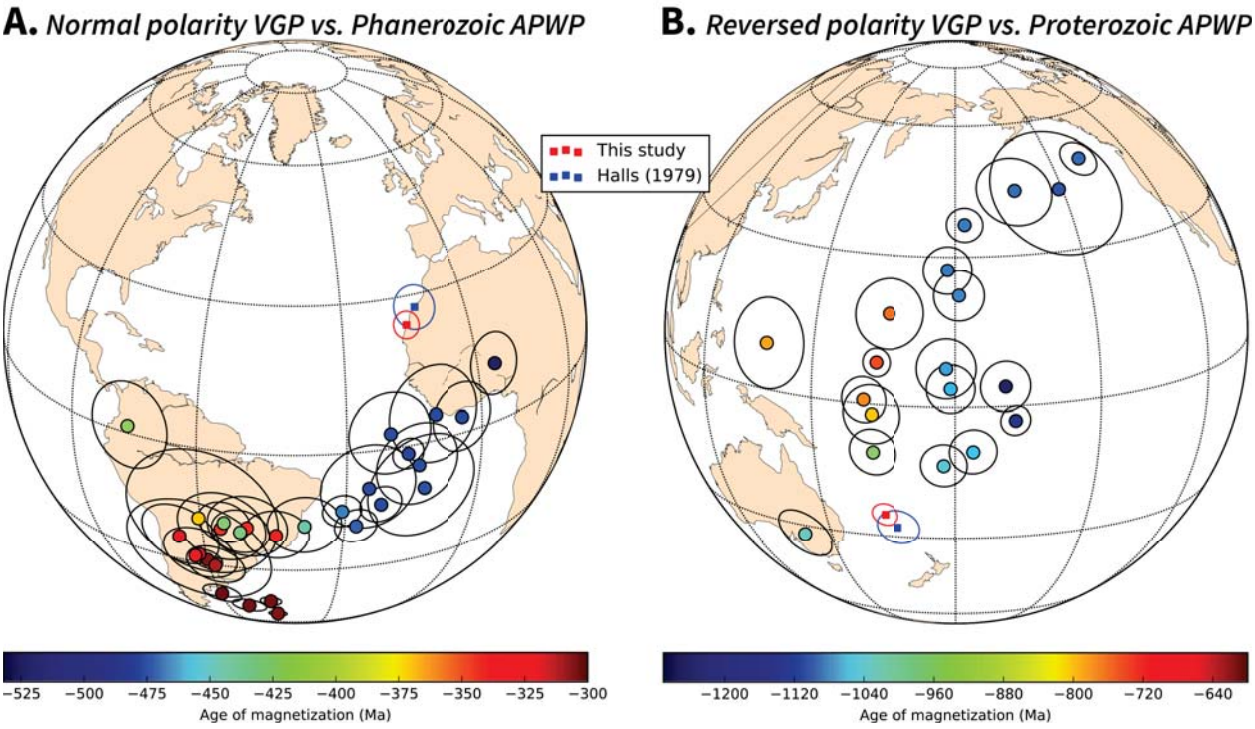

Figure S12. A) Comparison of Slate Islands VGP with the Phanerozoic APWP of Laurentia (Torsvik et al., 2012). The distance between the Slate Island VGP and the ca. 490 Ma Oneota Dolomite pole is 34.7°. The distance between the Slate Island VGP and the ca. 438 Ma Ringgold Gap pole is 46.8°. **B)** Comparison of Slate Islands VGP with the Proterozoic APWP of Laurentia.

3.3 Probability of a large deviation from geomagnetic north by a VGP

The statistical secular variation model TK03 (Tauxe and Kent, 2004) can be used to simulate secular variation with random draws being taken from the model. The function is set up to return directions so they are then recalculated as poles. Using this model, we can estimate the probability of there being a single VGP that is as far from the APWP path as the Slate Islands pole is from the Silurian path.

Distance from the Slate Islands to the 438 Ma Rose Hill pole can be calculated (colatitude) and used to determine the paleolatitude of the Slate Islands as constrained by the Rose Hill pole. This paleolatitude is then used for the latitude at which the random draw from the TK03 model are taken.

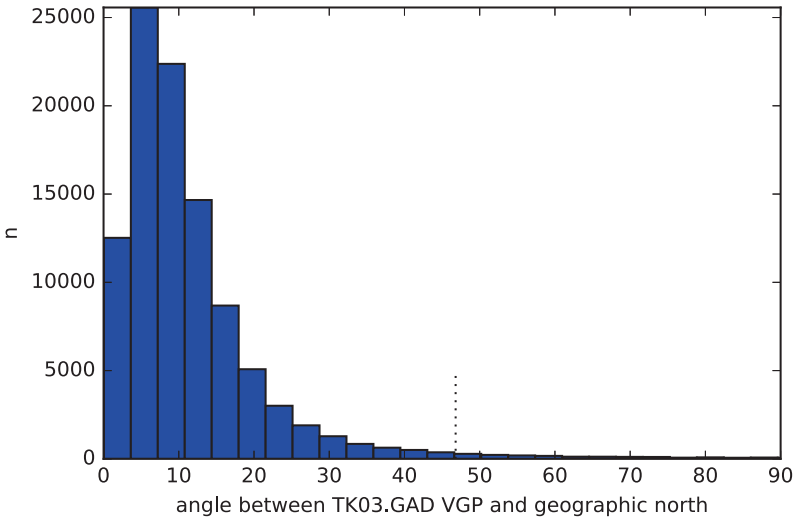

Figure S13. Distribution of poles from 100,000 draws from the TK03.GAD secular variation model (Tauxe and Kent, 2004). Approximately 5.7% of VGPs are >30° away from the mean pole, and about 3.3% of VGPs are >40° away from the mean pole. For reference, the degree of divergence of the Slate Islands VGP from the Silurian APWP is marked by the vertical dashed line.

4 Breccia Dike Cooling Model

4.1 Heat transfer during dike cooling

We are interested in modeling heat transfer during the emplacement and subsequent cooling of breccia dikes. We are particularly interested in understanding the timescale for cooling within the dike itself. This problem was dealt with nicely in an article published by Paul T. Delaney of the US Geological Survey.

4.2 An analytical solution to transient heat conduction

Delaney (1987) formulates the problem by idealizing a dike as a tabular plane of infinite extent. Coordinates are based on the position of the dike wall with the X-direction being the direction orthogonal to the wall such that negative X values are within the dike and positive X values are in the host rock. The dike has a thickness T and an initial temperature Θ_{mi} (subscript stands for magma initial). The host rock has an initial temperature Θ_{hi} and a thermal diffusivity κ_h. Conservation of energy for a motionless material undergoing one-dimensional heat transfer with no chemical reactions is (Carslaw and Jaeger, 1959, Ch. 1; Bird et al., 1960, Ch.10):

$$\rho C \frac{\partial \Theta}{\partial t} = \frac{\partial}{\partial X} k \frac{\partial \Theta}{\partial X} \tag{1}$$

This equation states that the heat conducted into a unit volume minus the heat conducted out is equal to the accumulation of heat within the volume. The right-hand side of equation 1 is the gradient in heat flux, which is given by Fourier's Law, $Q = -k\partial\Theta/\partial X$ where k is thermal conductivity; the left-hand side is the rate of accumulation of heat, where pC is heat capacity per unit volume. If k is constant, then:

$$\frac{\partial \Theta}{\partial t} = \kappa \frac{\partial^2 \Theta}{\partial X^2} \tag{2}$$

Thermal diffusivity, $\kappa = k/(pC)$, measures the ability of a material to conduct heat relative to its ability to accumulate heat.

Generality and simplicity are gained by introducing non-dimensional temperature θ, distance x, and time τ:

$$\theta = (\Theta - \Theta_{hi})/(\Theta_{mi} - \Theta_{hi}) \tag{3}$$

$$x = X/(T/2) \tag{4}$$

$$\tau = t * \kappa_h/(T/2)^2 \tag{5}$$

Following this introduction, Delaney (1987) builds up to presenting the first and simplest whole-time solution. This solution neglects thermal property contrasts between the host rock and dike (i.e. $\kappa_m/\kappa_h = 1$). These thermal property contrasts can affect the maximum temperatures reached in the host rock and early cooling rates, but the influence is rather small. This whole-time solution is:

$$\theta = \frac{1}{2}[erf\left(\frac{2+x}{\sqrt{4\tau}}\right) - erf\left(\frac{x}{\sqrt{4\tau}}\right)] \tag{6}$$

Delaney (1987) also presents numerical solutions that incorporate the effects of the heat of crystallization, magma flow and the temperature-dependence of thermal conductivity and diffusivity. In the application that we are exploring here, the cooling of a breccia dike emplaced within an impact crater neither the heat of crystallization nor magma flow apply and therefore the analytical solution using transient heat conduction theory will work well for our analysis.

4.3 Implementing the whole-time solution

4.3.1 Define the function dike_cooling()

A function can be defined that returns the temperature at a given time and distance from the contact (within or outside of the dike) for a given initial dike temperature, initial host rock temperature, dike width and thermal diffusivity (see code in digital notebook for details). This function calculates non-dimensional distance and time and then solves for non-dimensional temperature using the whole-time solution detailed above. The temperature of interest can then be extracted from the non-dimensional temperature using the specified initial temperatures.

4.3.2 Plot temperature vs distance at a number of times following dike emplacement

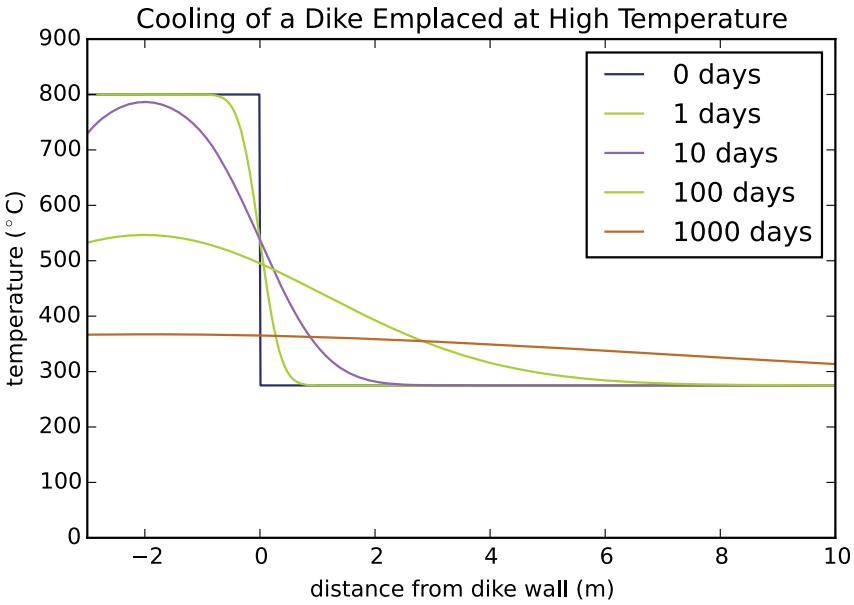

Figure S14. Temperature of a 4 meter-thick dike emplaced at 800 °C at different times post-emplacement.

4.3.3 Temperature dependence of thermal diffusivity

The above analysis does not incorporate the temperature-dependence of thermal diffusivity explored by Delaney (1987) in some detail. Laser flash-analysis has enabled advances in measurements of thermal diffusivity at elevated temperature since the work of Delaney (1987). Estimated of thermal diffusivity from schist, granite and rhyolite were published by Whittington et al. (2009).

These data were similar between the three rock types and the following empirical fits were proposed by Whittington et al. (2009) for the temperature dependence of thermal diffusivity (in square millimeters per second) in the continental crust.

$$\kappa_{crust}(T < 846K) = 567.3/T - 0.062 \tag{7}$$

$$\kappa_{crust}(T > 846K) = 0.732 - 0.000135T \tag{8}$$

Our temperature range of interest is between the estimated emplacement temperature of 800°C and the interval over which the majority of magnetite remanence will be blocked (580 to 400 °C). There is minimal fluctuation of thermal diffusivity over this temperature range in the empirical fit of Whittington et al. (2009). Figure S15 plots the Whittington et al. (2009) empirical fit over a range of temperature and calculates an average value over the temperature range of 800 °C to 400 °C for use in the cooling model.

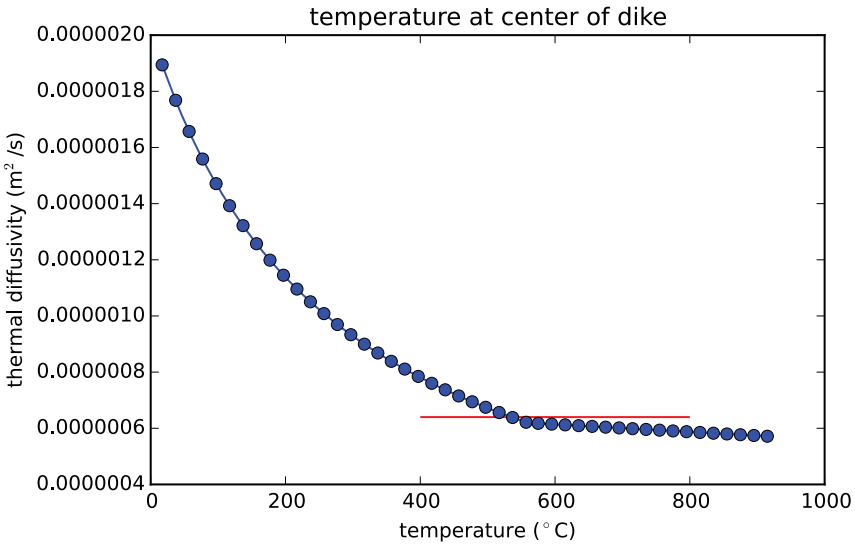

Figure S15. Thermal diffusivity as a function of temperature. The average thermal diffusivity in the range of 400–800 °C is plotted in red.

From this fit we obtain an average thermal diffusivity of $\kappa = 6.4{\times}10^{-7}\ m^2/s$ over the temperature range of interest for use in the model.

4.3.4 Implementing the Model

Because we would like to identify the minimum time over which the impact direction was acquired by a breccia dike after emplacement, we use the thinnest sampled breccia dike site (PI47; 4 cm thick) in the conductive cooling model. Paleomagnetic core samples from PI47 are 2.5 cm in diameter and therefore span most of the breccia dike's width as seen in the photo for the PI47 breccia dike in the paleomagnetic data analysis section. We therefore calculate characteristic cooling curves for both the center of the dike and 0.75 cm from the edge of the dike, since our paleomagnetic data encapsulates this range of positions within the PI47 breccia dike. The center of dike cools to 580 °C in 8.0 minutes, and 0.75 cm into the dike cools to 580 °C in 5.66 minutes. These cooling curves are shown in Figure 3 in the main text.

5 References

Delaney, P. T., 1987, Heat transfer during emplacement and cooling of mafic dykes: In Halls, H. and Fahrig, W., eds., Mafic dyke swarms, Geological Association of Canada, vol. 34, pp. 123–135.

Dressler, B. O., Sharpton, V. L., and Copeland, P., 1999, Slate Islands, Lake Superior, Canada: A mid-size, complex impact structure: Geological Society of America Special Papers, vol. 339, pp. 109–124, doi:10.1130/0-8137-2339-6.109.

Halls, H. C., 1979, The Slate Islands meteorite impact site: a study of shock remanent magnetization: Geophysical Journal of the Royal Astronomical Society, vol. 59, pp. 553–591, doi:10.1111/j.1365-246X.1979.tb02573.x.

Kirschvink, J., 1980, The least-squares line and plane and the analysis of paleomagnetic data: Geophysical Journal of the Royal Astronomical Society, vol. 62, pp. 699–718, doi:10.1111/j.1365-246x.1980.tb02601.x.

Swanson-Hysell, N. L., Maloof, A. C., Kirschvink, J. L., Evans, D. A. D., Halverson, G. P., and Hurtgen, M. T., 2012, Constraints on Neoproterozoic paleogeography and Paleozoic orogenesis from paleomagnetic records of the Bitter Springs Formation, Amadeus Basin, central Australia: American Journal of Science, vol. 312, pp. 817–884, doi:10.2475/08.2012.01.

Tauxe, L. and Kent, D., 2004, A simplified statistical model for the geomagnetic field and the detection of shallow bias in paleomagnetic inclinations: was the ancient magnetic field dipolar?: In Channell, J., Kent, D., Lowrie, W., and Meert, J., eds., Timescales of the paleomagnetic field, American Geophysical Union, vol. 145 of Geophysical Monograph, pp. 101–116, doi:10.1029/145GM08.

Tauxe, L., Shaar, R., Jonestrask, L., Swanson-Hysell, N., Minnett, R., Koppers, A., Constable, C., Jarboe, N., Gaastra, K., and Fairchild, L., 2016, PmagPy: Software package for paleomagnetic data analysis and a bridge to the Magnetics Information Consortium (MagIC) Database: Geochemistry, Geophysics, Geosystems, doi:10.1002/2016GC006307.

Torsvik, T. H., Van der Voo, R., Preeden, U., Mac Niocaill, C., Steinberger, B., Doubrovine, P. V., van Hinsbergen, D. J. J., Domeier, M., Gaina, C., Tohver, E., Meert, J. G., McCausland, P. J. A., and Cocks, L. R. M., 2012, Phanerozoic polar wander, palaeogeography and dynamics: Earth-Science Reviews, vol. 114, pp. 325–368, doi:10.1016/j.earscirev.2012.06.007.

Watson, G., 1956, A test for randomness of directions: Geophysical Journal International, vol. 7, pp. 160–161, doi:10.1111/j.1365-246X.1956.tb05561.x.

Whittington, A. G., Hofmeister, A. M., and Nabelek, P. I., 2009, Temperature-dependent thermal diffusivity of the Earth's crust and implications for magmatism: Nature, vol. 458, pp. 319–321, doi:10.1038/nature07818.